Magnetic ordering in manganese clusters

Mark B. Knickelbein
Chemistry Division, Argonne National Laboratory, Argonne, Illinois 60439, USA
(Received 5 November 2003; revised manuscript received 16 March 2004; published 22 July 2004)

Isolated manganese clusters, Mn_n, ($n=5-22$) are deflected by a linear-gradient magnetic field. Mn_7-Mn_{22} are found to deflect uniformly toward high field. The magnitude of the deflections indicate susceptibilities far in excess of those expected based on the susceptibility of bulk manganese, demonstrating that Mn clusters in this size range are magnetically ordered. Per-atom moments obtained from Curie's Law analysis range from $0.4\mu_b$ (Mn_{19}) to 1.7 μ_b (Mn_{12}). For Mn_5 and Mn_6, symmetric broadening of the cluster beam is observed, and their moments were determined via line-shape analysis using both free-spin and adiabatic rotor models. The measured moments, interpreted in light of recent density functional theory calculations, suggest that Mn clusters in this size range are molecular ferrimagnets.

DOI: 10.1103/PhysRevB.70.014424 PACS number(s): 36.40.Cg, 75.50.Tt, 39.10.+j, 82.80.Rt

I. INTRODUCTION

Due to the effects of spatial confinement, clusters and small nanoparticles composed of transition metal atoms can, like ultrathin films,[1] exhibit magnetic ordering not displayed by the corresponding bulk solids. For example, using a molecular beam deflection technique Cox and coworkers showed that bare rhodium clusters ($Rh_{9\text{-}60}$) display magnetic moments[2,3] as high as 0.8 μ_b per atom (Rh_9-Rh_{11}) indicative of ferromagnetic or ferrimagnetic ordering, even though bulk rhodium is a Pauli paramagnet at all temperatures.[4] The same group also measured magnetic moments for Cr_8-C_{156} that ranged from $\sim$0.5 to $\sim$1.0 μ_b per atom, values far larger than would be expected if these clusters displayed antiferromagnetic ordering as in bulk chromium.[5] Recently, de Heer has coworkers have found evidence for magnetic ordering in palladium clusters.[6]

Below its Néel temperature of 95 K, α-manganese is antiferromagnetically ordered and is paramagnetic above 95 K.[4,7,8] However, the large paramagnetic susceptibility displayed by bulk Mn ($\chi_g=9.6\times10^{-6}$ cm^3g^{-1} for α-Mn at 0 K)[4] suggests that it is on the verge of ferromagnetic instability, as predicted by the Stoner model.[9,10] In a previous paper we showed that molecular beams of manganese clusters in the size range $Mn_{11}-Mn_{99}$ produced at 68 K display substantial high-field deflections in an inhomogeneous magnetic field.[11] The magnitude of these deflections were one to two orders of magnitude larger than would be expected if the clusters possessed susceptibilities characteristic of either antiferromagnetic or paramagnetic bulk manganese, indicating that manganese clusters in this size range possess an ordering of spins that results in per-atom moments $\overline{\mu}$ ranging from $\sim$0.3 to over 1 μ_b per atom.[11] We have extended our measurements to smaller manganese clusters, and in this paper we present the results of molecular beam deflection measurements for Mn_5-Mn_{10}, along with refined results for the $Mn_{11}-Mn_{22}$ range. We find that, like the larger Mn clusters examined in our previous study, smaller Mn clusters also display anomalously large susceptibilities resulting from magnetic ordering. Recent density function theory (DFT) calculations indicate that the ground state isomers of small manganese clusters tend to be ferrimagnetically ordered.[12–14] Our present results are in accord with these predictions.

II. EXPERIMENTAL METHODS

The experimental methods have been previously provided in detail.[15] The experiment was performed using a four-stage, differentially pumped molecular beam apparatus, shown in Fig. 1. Manganese clusters were produced via pulsed laser vaporization of a cylindrical manganese target (99.99%, Ames Materials Preparation Center, Ames, Iowa[16]) through which helium was flowed continuously. The laser vaporization source was coupled to a high aspect ratio flow tube (9 cm length $\times$ 0.3 cm diameter) held at 68 ± 2 K.[17] The residence time of the clusters within the flow tube ($\sim$4 ms) was sufficient to ensure that they were equilibrated to the flow tube temperature prior to expansion into vacuum.[18] At the helium flow rates used ($\sim$1000 sccm), the pressure within the flow tube was 10 ± 1 Torr. The clusters expanded into vacuum through a 1.0 mm diameter orifice at the end of the flow tube. Under these mild expansion conditions, very little supersonic cooling of the clusters' vibronic degrees of freedom is expected,[19] so that the post-expansion cluster temperature is estimated to be close (within $\sim$5 K) to that of the flow tube. The expanding jet was skimmed into a molecular beam, which passed through a gradient dipole magnet[20] capable of producing B fields of up to $\sim$1.2 T and gradients ($\partial B/\partial z$) up to $\sim$210 T m^{-1} in the center of the gap. The clusters were then ionized with a spatially expanded ArF excimer laser ($\lambda=193$ nm), with the resulting singly ionized clusters detected via position-sensitive time-of-flight (PSTOF) mass spectrometry[15,21] 0.9 m downbeam of the magnet exit slit. This technique allows the spatial distributions of clusters in a molecular beam to be mapped onto the time-domain and thus recorded using a digital oscilloscope. The spatial deflections or broadening of each cluster size in the beam was independently measured by quantitatively comparing the field on versus field off PSTOF peak profiles as described below.

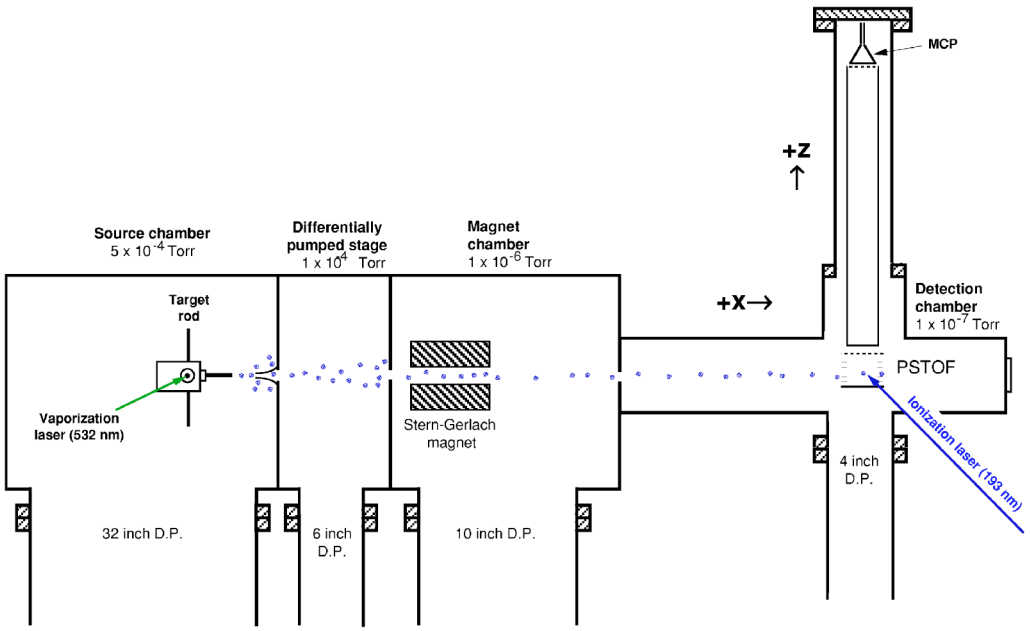

FIG. 1. (Color online) The molecular beam deflection apparatus.

III. RESULTS AND DISCUSSION

A. Magnetic Moments

Magnified portions of the TOF spectrum, showing Mn_6 and Mn_8 mass peaks recorded with the deflection field off versus on, are shown in Fig. 2. At nonzero fields, two types of deflection behavior, exemplified in Fig. 2, are observed. The PSTOF mass peaks of Mn_5 and Mn_6 broaden symmetrically about the undeflected center line of the beam ($z=0$), with no net deflection in the z direction. By contrast the TOF peaks for Mn_7 and larger clusters shift uniformly to later arrival times upon application of the gradient field, corresponding to a net spatial shift in the $+z$ direction toward higher fields, as quantified using the PSTOF peak average position, (i.e., their first moments). This high field-seeking behavior, displayed by Mn_7 and larger Mn clusters, has been observed in previous molecular beam deflection studies of Fe_n (Refs. 22–25), Co_n (Refs. 24,26,27), Ni_n (Refs. 15,23,24,28,29), and Rh_n (Refs. 2,3) and is consistent with superparamagnetic behavior, indicating that intramolecular spin relaxation occurs on a time scale shorter than the flight time of the clusters through the magnetic field ($\sim$0.4 ms). Spin relaxation in isolated clusters can occur only if their rovibronic densities of states are sufficiently large that the clusters can serve as their own heat baths. Khanna and Linderoth recognized that in this situation, a thermodynamic analysis can be brought to bear via the Langevin model of paramagnetic susceptibilities[30] (*vide infra*).

By contrast, symmetric broadening of the PSTOF peaks, as observed for Mn_5 and Mn_6, suggests either that spin-relaxation does not occur (*free-spin* behavior, as is the case for isolated atoms and small molecules) or that the magnetic moments of these clusters are strongly coupled to their atomic frameworks (via magnetocrystalline or other type of anisotropy) and thus rotate with the clusters as a whole. The latter locked moment behavior, observed in magnetic deflection studies of lanthanide clusters by Douglass *et al.*,[27,31] Cox *et al.*,[32] and Bucher and Bloomfield[33] results in a field-

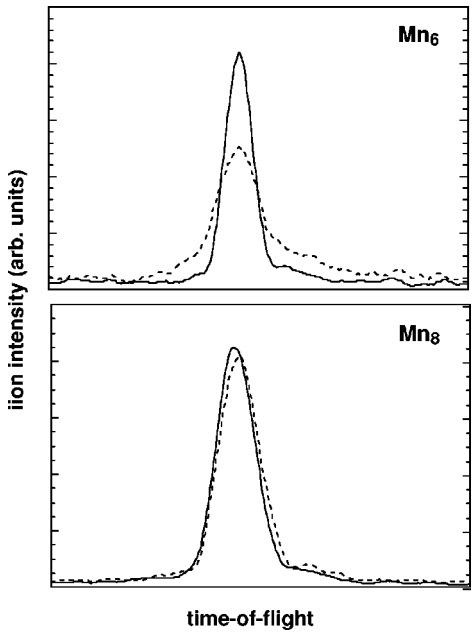

FIG. 2. A magnified view of the manganese cluster time-of-flight spectrum showing the PSTOF profiles for Mn_6 and Mn_8. The PSTOF mass peaks shown here were numerically smoothed for illustrative purposes. Solid traces: B, $\partial B/\partial z=0$; dashed traces: $B=0.97$ T, $\partial B/\partial z=192$ T m^{-1}. The slight asymmetry of the field-broadened peak is due to slight z-dependent variations in the ion collection efficiency of the PSTOF mass spectrometer. Actual measurements of the magnetic moments of Mn_5 and Mn_6 were performed at significantly lower gradients than employed in this example, in the regime of uniform ion collection efficiency.

induced broadening of the cluster beam akin to that displayed by beams of polar molecular in inhomogeneous electric fields.[34] In the analysis of the field-induced beam broadening for Mn_5 and Mn_6, we will consider both free spin behavior and locked moment behavior.

1. Mn_5 and Mn_6

As shown in Fig. 2, a beam of Mn_6 clusters which passes through a gradient field undergoes a symmetric broadening about $z=0$; Mn_5 behaves similarly. One plausible mechanism for such beam broadening is simple free-spin behavior of an angular momentum J system, whereby the beam would spatially separate into $2J+1$ equally spaced (but unresolved) beamlets, as is observed in Stern-Gerlach deflection studies atoms and small molecules having nonzero electronic angular momentum.[35] At the PSTOF detector these beamlets, each corresponding to a distinct magnetic quantum number m_J, would display deflections ranging from $-z_{\max}$ to $z_{\max}$, with the most strongly deflected beamlets corresponding to $m_J=\pm J$. The z_{m_j} values are given by

$$z_{m_j}=\frac{gm_j\mu_b LD}{mv^2}\left(\frac{\partial B}{\partial z}\right), \tag{1}$$

where g is the molecular g-factor particular to the system, μ_b is the bohr magneton (9.273×10^{-24}J T^{-1}), L is the length of the magnet, and D is the distance from the final collimating slit to the detector.[15] Knowledge of $z_{\max}$ would lead directly to the z component of the vector magnetic moment of the system, given as $\mu=gJ$ [see Eq. (1)], however because the individual beamlets are not spatially resolved, $z_{\max}$ must be extracted from the observed field-induced broadening of the beam. It is shown in the Appendix that for a free-spin system the hypothetical field-broadened peak shape Q^{FS} is, in the limit of infinite J, a function of $z_{\max}$ approximated by the following convolution with the unbroadened (zero-field) spatial distribution $P(z)$:

$$Q^{\mathrm{FS}}(z_0,z_{\max})=\frac{1}{2z_{\max}}\int_{z_0-z_{\max}}^{z_0+z_{\max}}P(z)dz. \tag{2}$$

The desired quantity $z_{\max}$ is obtained by fitting Q^{FS} to the experimentally measured field-broadened PSTOF peak. In practice, this was done by variation of $z_{\max}$ until the rms difference between the measured field-broadened peak and Q^{FS} was minimized. It is demonstrated in the Appendix that the values of $z_{\max}$ obtained by this procedure [and thus the magnetic moments, obtained via Eq. (1)] are upper limits to the actual values, with the accuracy of the approximation improving with increasing J. The accuracy of this semiclassical model has been verified in Stern-Gerlach beam deflection studies of atomic terbium (ground state term $^6H^0_{15/2}$, $\mu_z=10\ \mu_b$).[36] An example showing the zero-field and field-broadened PSTOF profiles of Mn_6, along with the best-fit convolution assuming free-spin behavior is shown in Fig. 3. Applying this fitting procedure to profiles measured at several values of the field gradient, we find that Mn_5 possesses a moment $\bar{\mu}$ of $0.48\pm0.20\ \mu_b$ per atom, while Mn_6 possesses a moment of $0.35\pm0.15\ \mu_b$ per atom. The relatively large uncertainty reported for the magnetic moments of these smaller clusters reflects poor signal-to-noise ratios resulting from their low abundances in the beam. As noted above, these values of $\bar{\mu}$ represent upper limits to the true moments and because the moments (and thus the corresponding angular momenta J) are relatively small, we can expect that the overestimation for the moments of Mn_5 and Mn_6 may be as high as 20–40%, depending on J (see the Appendix).

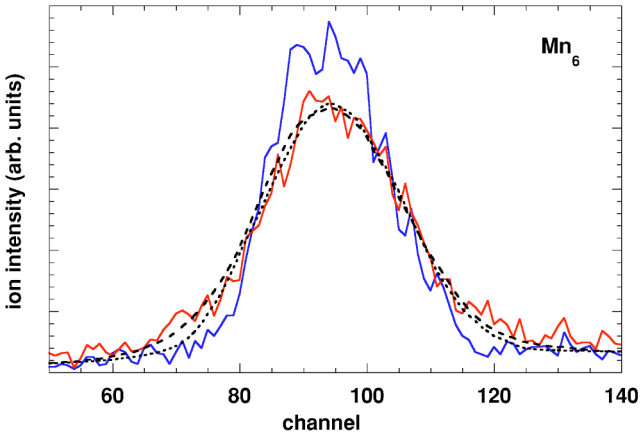

FIG. 3. (Color online) Unbroadened and field-broadened PSTOF profile for Mn_6 (solid curves), along with the rms best fit convolutions Q^{FS} (fine dashed curve) and Q^{AR} (coarse dashed curve). The abscissa is in units of oscilloscope channels, 2 ns per channel.

The beam-broadening displayed by Mn_5 and Mn_6 can also be interpreted within the framework of locked-moment behavior, in which the magnetic moment of each cluster rotates with the cluster as it tumbles through the magnet. In their *adiabatic rotor* treatment, Bertsch and Yabana treated locked-moment magnetic clusters as thermal ensemble of spherical rotors (rotational temperature T_{rot}) each possessing a rigidly fixed moments of magnitude μ.[37] Their analysis showed that in the limit of low fields ($\mu B\ll kT_{\mathrm{rot}}$), the distribution of the z component of magnetation $R(\mu_z)$ is given by

$$R(\mu_z)=\frac{1}{2\mu}\ln\left(\frac{\mu}{|\mu_z|}\right). \tag{3}$$

Unlike the flat, square-sided distribution δ assumed for the semiclassical model of free spins (see the Appendix), $R(\mu_z)$ is strongly peaked at $\mu_z=0$, and decays asymptotically to zero at $\mu_z=\pm\mu$.

Before applying the adiabatic rotor model we must consider the validity of the weak-field assumption $\mu B\ll kT_{\mathrm{rot}}$. The jet expansion conditions used in the present experiments (stagnation pressure ~10 Torr, nozzle diameter 0.1 cm, stagnation temperature 68 K) are such that the terminal translation temperature T_{trans} in the beam is predicted to be of the order of 1 K.[38] Experimentally it has been found[39,40] that heavy molecules generally do not undergo efficient rotational cooling in helium expansions however, due to velocity slip effects, such that the rotational temperatures are typically closer to the stagnation pressure than to T_{trans}. For locked-moment clusters studied under conditions in which $\mu B\approx kT_{\mathrm{rot}}$, theory predicts[37,41–45] and experiments show[27,31,33] that beam broadening is accompanied by a measurable high-

field shift in the spatial distribution of the cluster beam; the magnitude of this shift increases with increasing field. No such shifts are observed for Mn_5 and Mn_6 in the present experiment, however. It is concluded that $\mu B \ll kT_{rot}$ is a valid assumption so that we may use Eq. (3) extract moments for Mn_5 and Mn_6 using the locked moment-adiabatic rotor model. This was done by convoluting the unbroadened PSTOF peak profile $P(z)$ with the distribution function R in a similar fashion as was done in the free-spin case [see Eq. (2)]:

$$Q^{AR}(z_0, z_{max}) = \int_{z_0 - z_{max}}^{z_0 + z_{max}} P(z) R(z - z_0) dz. \quad (4)$$

[Because we are modeling spatial distributions rather than the z-distribution of moments, the argument of the distribution function R has been changed from μ_z to $z - z_0$. These variables are linearly related to one another via Eq. (1).] Moments were obtained by minimizing the rms difference between the experimental field-broadened peak and the assumed distribution Q^{AR} by varying z_{max}, which in this case corresponds to the deflection distance of clusters with $\mu_z = \pm\mu$. An example of a best-fit adiabatic rotor convolution Q^{AR} for Mn_6 is shown in Fig. 3 along with the free-spin result Q^{FS}. The adiabatic rotor model applied to PSTOF profiles recorded at various fields yields $\overline{\mu} = 0.79 \pm 0.25\ \mu_b$ for Mn_5 and $\overline{\mu} = 0.55 \pm 0.10\ \mu_b$ for Mn_6.

Both models adequately reproduce the broadened PSTOF profiles obtained at relatively low fields, with the adiabatic rotor model yielding somewhat higher moments than the free-spin model. However for significantly broadened peaks obtained at high field, the adiabatic rotor model is consistently superior at reproducing the wings of the distributions (see Fig. 3). Based on the line-shape analyses, it is concluded that Mn_5 and Mn_6 are locked moment clusters. Accordingly, we report the values of $\overline{\mu}$ for Mn_5 and Mn_6 obtained via the adiabatic rotor model in Table I. It is shown below that even with large uncertainties due to experimental noise, values of $\overline{\mu}$ can be determined for Mn_5 and Mn_6 with sufficient accuracy to identify isomers among several candidates having widely varying moments.

2. Mn_7–Mn_{22}

The induced magnetization values $\langle M_z \rangle$ of the ensembles of clusters displaying high field-seeking behavior were calculated from the magnitude of the deflection Δz (as computed from the change in TOF mass peak first moments), the molecular beam speed v and $\partial B / \partial z$ via,[15,23,33]

$$\langle M_z \rangle = \frac{\Delta z m v^2}{LD} \left(\frac{\partial B}{\partial z} \right)^{-1}, \quad (5)$$

where m is the cluster mass, L is the length of the deflection magnet, and D is the distance from the final collimating slit to the photoionization region of the PSTOF mass spectrometer. The magnetization per atom for $Mn_{7\text{-}22}$ determined from the measured deflections via Eq. (5) was found to increase linearly with magnetic field up to $B = 0.5$ T, above which instrument-related nonlinearities were observed for strongly deflected clusters. The per-atom (dimensionless[46]) susceptibilities χ, derived from $\langle M_z \rangle$ measured at $B = 0.425$ T are shown in Fig. 4. The susceptibilities span the range $\sim 11\,000 \times 10^{-6}$ (Mn_{19}) to $\sim 184\,000 \times 10^{-6}$ (Mn_{25}). By comparison, the per-atom susceptibility of bulk, solid manganese lies 1–2 orders of magnitude lower, ranging from 790×10^{-6} (α-manganese at ~ 900 K) to 1220×10^{-6} (δ-Mn at 1500 K).[4] These results clearly suggest that at 68 K manganese clusters possess magnetic properties that are fundamentally different from any known phase of bulk manganese.

TABLE I. Magnetic moments (per atom) for Mn_n.

n	moment (μ_b)	±
5	0.79	0.25
6	0.55	0.10
7	0.72	0.42
8	1.04	0.14
9	1.01	0.10
10	1.34	0.09
11	0.86	0.07
12	1.72	0.04
13	0.54	0.06
14	1.48	0.03
15	1.66	0.02
16	1.58	0.02
17	1.44	0.02
18	1.20	0.02
19	0.41	0.04
20	0.93	0.03
21	1.20	0.02
22	1.16	0.02

For an ensemble of magnetically ordered clusters possessing total electronic angular momentum J, application of a magnetic field B leads to a splitting into $2J+1$ magnetic sublevels.[10] However unlike the situations for magnetic at-

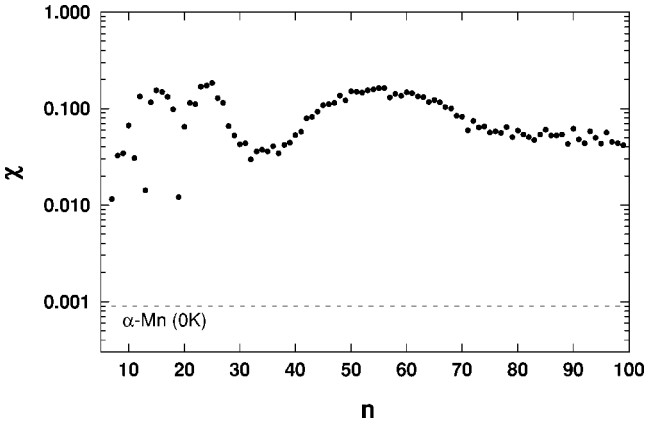

FIG. 4. Per-atom susceptibilities χ for Mn_7-Mn_{22} derived from low-field measurements of cluster magnetization $\langle M_z \rangle$. The per-atom susceptibility of α-manganese at 0 K is shown by the dashed line.

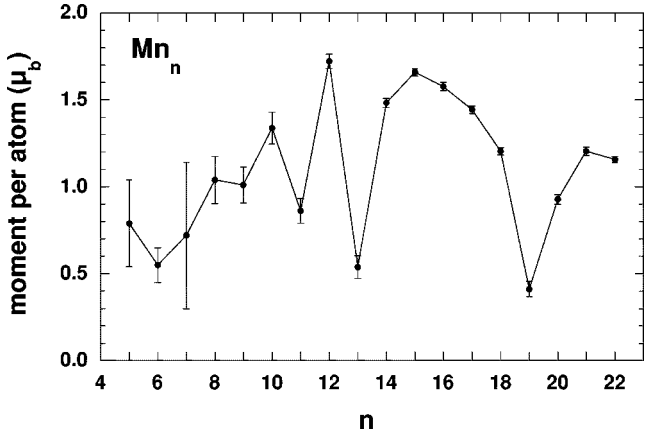

FIG. 5. Magnetic moments per atom $\bar{\mu}$ of Mn_5-Mn_{22}. Values shown for Mn_5 and Mn_6 were obtained using the adiabatic rotor model (see the text).

oms, the densities of states in the larger Mn_n clusters are sufficiently large that transitions between the $2J+1$ sublevels (i.e., spin-relaxation) occur rapidly. If these transitions facilitate a thermal equilibrium among the $2J+1$ Zeeman sublevels, then the "sample" of clusters will be magnetized with magnetization $\langle M_z \rangle$ as determined by the thermodynamic average of the z components of the intrinsic magnetic moment $\mu_z = gJ_z\mu_b$

$$\langle M_z \rangle = \mu_{\text{cluster}} B_J(y), \tag{6}$$

where $B_J(y)$ is the Brillouin function, given by

$$B_J(y) = \left(\frac{2J+1}{2J}\right)\coth\frac{(2J+1)y}{2J} - \left(\frac{1}{2J}\right)\coth\frac{y}{2J},$$

with $y = \mu_{\text{cluster}} B/kT$. At temperatures in which $\mu_{\text{cluster}} B \ll kT$, as is the case in this and similar molecular beam experiments, $\langle M_z \rangle$ varies quadratically with the cluster magnetic moment (the Curie Law)

$$\langle M_z \rangle \approx \frac{\mu^2_{\text{cluster}} B}{3kT} = \frac{n^2 \bar{\mu}^2 B}{3kT}. \tag{7}$$

This expression is appropriate for situations in which the magnetocrystalline anisotropy energy is negligible compared to kT, and has been used to analyze magnetic deflection measurements of transition metal clusters produced at temperatures where its validity applies.[23,30,33,47]

The mean per-atom magnetic moments $\bar{\mu}$, determined for $Mn_{7\text{-}22}$ using the Curie's Law expression given above, are shown in Fig. 5 together with the values obtained above for Mn_5 and Mn_6. Efforts at improving the production efficiency of small clusters has resulted in significantly improved signal-to-noise ratios and thus more reliable magnetic moment determinations for clusters in the $n=11-22$ range, as compared to those reported in our preliminary paper.[11] In particular, the present values for Mn_{11} and $Mn_{14\text{-}16}$ are somewhat higher than those previously reported. The values for the other clusters in this range are generally (within overlapping error bars) approximately the same as those previously reported.[11]

B. Comparison to Electronic Structure Calculations

Several density functional theory (DFT) calculations of the optimized structures and magnetic properties of manganese clusters have been published.[12–14,48–51] For any given cluster size, such calculations generally reveal several nearly isoenergetic isomers, making definitive identification of the actual ground state structures difficult. However, because the isomers often display widely varying magnetic moments, the experimentally determined values can be used to identify the isomer actually produced in the experiment or at least to rule out unlikely candidates. It is possible that multiple isomers are also produced in the experiment in which case the elucidation of structures by comparing experiment and theory is much less straightforward. Threshold photoionization experiments, for example, have provided evidence that Mn_{13} is produced in two isomeric forms when generated in a laser vaporization source similar to that used in the present magnetic deflection studies.[17]

1. Mn_5

Electron spin resonance studies by Van Zee *et al.*[52] and Baumann *et al.*[53] have shown that matrix-isolated Mn_5 is a high-spin molecule with $S=25/2$ resulting from ferromagnetic coupling of spins, and thus a per-atom moment of $5\mu_b$. This value is in reasonable accord with trigonal bipyramidal (tbp) ground state structures found in DFT studies by Pederson, Reuss, and Khanna (PRK)[48] (4.6 μ_b per atom), and by Nayak and Jena[49] (5 μ_b per atom), but is considerably larger than the value of 0.8 ± 0.3 μ_b measured in the present experiment, implying that different isomers were produced in the two experiments. Bobadova-Parvanova, Jackson, Srinivas, and Horoi (BJSH)[13] and Jones, Khanna, Baruah, and Pederson (JKBP)[54] have found a tbp-like structure (Fig. 6) having a per-atom moment of 0.6 μ_b as the ground state, in reasonable agreement (within experimental error) with the value determined in the present study. Another tbp isomer with $\bar{\mu}=4.6$ μ_b and lying slightly higher in energy was also identified by both BJSH and by JKBP.

2. Mn_6

For Mn_6, PRK[48] considered octahedral and pentagonal pyramid structures and found moments of 4.33 μ_b and 4.66 μ_b per atom, respectively, considerably larger than our measured value. BJSH have reported five nearly isoenergetic structures for Mn_6—four having octahedronlike structures and a bicapped tetrahedron.[13] The ground state found in that study was an octahedron with $\bar{\mu}=1.33$ μ_b per atom. The next three higher-lying isomers (also octahedral) possess per-atom moments of 4.33 μ_b ($\Delta E=+0.03$ eV), 2.66 μ_b ($\Delta E=+0.03$ eV), and 0.33 μ_b ($\Delta E=+0.08$ eV). The bicapped tetrahedron ($\Delta E=+0.08$ eV) was found to possess a moment of 1.33 μ_b per atom. JKBP[54] have also identified several nearly isoenergetic structures for Mn_6, all octahedral-like, with $\bar{\mu}=1.33$ μ_b (ground state), 2.66 μ_b ($\Delta E=+0.03$ eV), 4.33 μ_b ($\Delta E=+0.03$ eV), and 0.33 μ_b ($\Delta e=+0.06$ eV). Our measured value of $\bar{\mu}=0.6\pm0.1$ μ_b, lies between that of the $\bar{\mu}=0.33$ μ_b isomer (Fig. 6) and the $\bar{\mu}=1.33$ μ_b ground state isomer, although it is closer to the former. It is conceivable

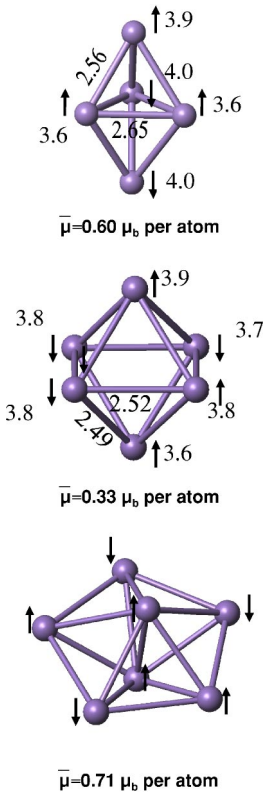

FIG. 6. (Color online) Ground state structures of Mn_5 (Refs. 13 and 54), Mn_6 (Refs. 13 and 54), and Mn_7 (Ref. 14) as determined by DFT studies. Local atomic moments (in units of μ_b, obtained by integrating spin density within nonoverlapping spheres centered on each atom) and typical bond lengths (Å) are shown for Mn_5 and Mn_6. Corresponding values for Mn_7 are similar (Ref. 56).

that multiple isomers are produced in this experiment, such that the measured value is an average of the 0.33 μ_b isomer and one or more of the higher-moment isomers.

3. Mn_7

BJSH[13] and Khanna, Rao, Jena, and Knickelbein[14] (KRJK) have reported three pentagonal bipyramid (pbp) structures as the lowest lying isomers of Mn_7. Although the spin arrangements of the ground state structures found by BJSH and KRJK differ slightly from one another, they are both ferrimagnetically ordered pbp-like structures with $\bar{\mu} = 0.71\ \mu_b$ per atom (Fig. 6), in good agreement with the experimentally determined value of $0.72 \pm 0.42\ \mu_b$. Although there is disagreement in the reported moments found for the next two higher-lying pbp isomers, their moments are several times higher than the experimental value, eliminating them from consideration as ground state candidates. PRK[48] investigated several trial structures (including pbp) and found them to be ferromagnetic, with moments significantly higher than that measured in the present study.

4. Mn_{13}

Our previous photoionization studies[17] have suggested that Mn_{13} may be produced in (at least) two isomeric forms, in which case the experimentally measured moment ($\bar{\mu} = 0.54 \pm 0.06\ \mu_b$) is an average value weighted according to the relative abundances of the isomers in the beam—quantities that cannot be determined with high precision. Nayak, Nooijen, and Jena[51] found three isomers for Mn_{13}: icosahedral (ground state, $\bar{\mu} = 2.54\ \mu_b$ per atom), hexagonal-like ($\Delta E = +0.05$ eV, 1.31 μ_b per atom), and cuboctahedral ($\Delta E = +0.44\ E$, $0.39 \mu_b$ per atom). Although the cuboctahedron was considerably higher in energy than the ground state icosahedron, its predicted magnetic moment of $0.39 \mu_b$ per atom lies closer to the experimentally determined value than the other isomers considered in that DFT study. Both Briere, Sluiter, Kumar, and Kawazoe (BSKK)[12] and BJSH,[13] found several icosahedral minima for Mn_{13}. In both studies, the ground state was found to be a ferrimagnetic icosahedron with a per-atom moment of 0.23 μ_b. The next higher-lying isomer found by BJSH,[13] also a ferrimagnetic icosahedron, was found to possess a moment of 0.54 μ_b per atom, in quantitative agreement with the value measured in the present study. Other icosahedral minima were also found in both studies, with considerably higher moments—up to 4.38 μ_b per atom for one ferromagnetic solution.[13]

5. Larger Mn_n

BSKK also examined selected larger clusters.[12] For Mn_{15}, both body-centered cubic (bcc) and icosahedral minima were found. The per-atom moment of the lowest-energy icosahedral structure was 0.60 μ_b, while that of the lowest-lying bcc structure was 0.20 μ_b, both well below the measured value of $1.66 \pm 0.02\ \mu_b$. Higher-lying Mn_{15} isomers possessing moments nearer the experimental value were found in this study, however. For Mn_{19}, BSKK found the minimum structure to be a ferrimagnetic double icosahedron with a per-atom moment of 1.21 μ_b, considerably higher than the experimentally determined value of 0.41 μ_b. For Mn_{23}, the triple icosahedron was found to be the lowest-lying isomer, with a moment of 0.91 μ_b per atom. The experimental value previously reported for Mn_{23} is $1.24 \pm 0.05\ \mu_b$ per atom.[11]

Taken together, the various DFT calculations of Mn cluster structures and magnetic properties cited above account for the magnitude of the measured magnetic moments overall. In particular, while the local atomic moments are typically in the 3.5–4 μ_b range (e.g., see Fig. 6), the propensity toward antiferromagnetic ordering among the spins leads to ferrimagnetic structures, typically having net moments of $\sim 1\ \mu_b$ per atom or less (with a few exceptions, such as Mn_{12}). While these theoretical studies have provided a basic understanding of the magnetic ordering in small Mn clusters, additional studies of larger Mn clusters will be required in order to understand the rich oscillatory structure exhibited in the Mn_{10}–Mn_{99} range.[11]

ACKNOWLEDGMENTS

The author thanks Professor Alan Jackson, Dr. Julius Jellinek, Professor Puru Jena, Professor Shiv Khanna, and Professor Sudha Srinivas for informative discussions regarding their DFT calculations of Mn cluster structures. This work is supported by the U.S. Department of Energy, Office of Basic

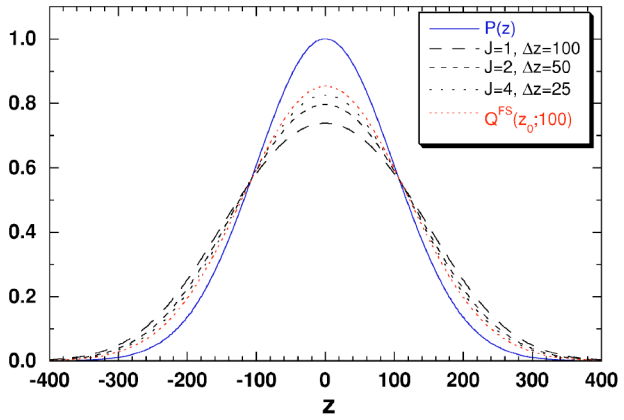

FIG. 7. (Color online) $P(z)$ and $Q^{\mathrm{FS}}(z_0;100)$ along with sum-of-gaussians distributions for $J=1$, 2, and 4. As $J\rightarrow\infty$, the sum-of-gaussians distribution converges to Q^{FS} (see the text).

Energy Sciences, Division of Chemical Sciences, under Contract W-31-109-ENG-38.

APPENDIX

Consider a beam of atoms or molecules of mass m and angular momentum J traveling with a speed v along the $+x$ direction. The beam is assumed to have a finite spatial width w in the $\pm z$ direction, transverse to the direction of travel but parallel to the gradient of the Stern-Gerlach magnet through which the beam passes (see Fig. 1). In a magnetic deflection experiment in which spin relaxation does not occur and in which the angular momentum is not coupled to the molecular framework (i.e., the free-spin limit), the beam will spread into $2J+1$ beamlets having values of $m_j=-J,-J+1\ldots J-1,J$ after passing through the gradient field. At the detector, each beamlet is displaced by an amount z_{m_j} from the undeflected ($z=0$) position proportional to its value of m_j [see Eq. (1)]. In an ideal experiment with an infinitely thin molecular beam ($w\rightarrow 0$), the $2J+1$ beamlets are resolved at the detector and the magnetic moment of the system $\mu=g[J(J+1)]^{1/2}$ can be determined directly from the values of g and J obtained from the spatial deflection pattern.

However in the case of a molecular beam with w significantly greater than the spacing between the beamlets, the individual beamlets are not resolved and the magnetic moment must be determined indirectly by analyzing the broadening of the beam. In what follows $P(z)$ represents the spatial distribution (i.e., the shape) of the unbroadened TOF peak measured with the magnetic field off, and Q^{FS} is the distribution of the broadened peak. Q^{FS} can be represented as the convolution of $P(z)$ with some function δ that accounts for the spatial broadening along the $\pm z$ directions

$$Q^{\mathrm{FS}}(z_0)=\int_{-\infty}^{\infty}P(z)\delta(z-z_0)dz. \tag{A1}$$

In reality, $\delta(z-z_0)$ is akin to a "picket fence," namely, a sum of $2J+1$ evenly spaced Dirac delta functions, each multiplied by $(2J+1)^{-1}$ so as to maintain conservation of the total peak area. However because for the field-broadened distribution neither the number of beamlets (determined by J) nor their spacing (determined by g) is known, we shall make the simplifying assumption that $\delta(z-z_0)$ is constant over an interval whose width is equal to $2z_{\mathrm{max}}$, a distance that corresponds to two times the deflection of the two most strongly deflected beamlets, (i.e., those with $m_J=\pm J$):

$$\begin{aligned}\delta(z-z_0)&=0, \quad z-z_0<-z_{\mathrm{max}}\\ &=\frac{1}{2z_{\mathrm{max}}}, \quad -z_{\mathrm{max}}\leqslant z-z_0\leqslant z_{\mathrm{max}}\\ &=0, \quad z-z_0>z_{\mathrm{max}}.\end{aligned} \tag{A2}$$

Note that the integrated area under this function is 1, as required to conserve the total area of the distribution after convolution. Equations (A2) together comprise one of the operative definitions of the Dirac δ function.[55] With this definition of $\delta(z-z_0)$, Eq. (A1) becomes

$$Q^{\mathrm{FS}}(z_0,z_{\mathrm{max}})=\frac{1}{2z_{\mathrm{max}}}\int_{z_0-z_{\mathrm{max}}}^{z_0+z_{\mathrm{max}}}P(z)dz. \tag{A3}$$

In practice $P(z)$ is known numerically but not analytically, so that numerical integration must be employed to evaluate Q^{FS}. An example of the application of Eq. (A3) assuming $z_{\mathrm{max}}=100$ (arbitrary units) is shown in Fig. 7. The unbroadened peak $P(z)$ was assumed to have a gaussians shape (a mathematically convenient choice but one that also represents the actual PSTOF mass peak shapes reasonably well). Shown in Fig. 7 along with $P(z)$ and Q^{FS} are distributions representing the sums of 3, 5, and 9 equally spaced gaussian functions corresponding to $J=1,2$, and 4, respectively. Each individual gaussian function has the same width as $P(z)$ and the resulting sum-of-gaussians function was scaled by $(2J+1)^{-1}$ as required to satisfy conservation of intensity. The spacing Δz between the individual gaussians in the sum-of-gaussians distributions were chosen to be proportional to z_{max}/J so that those individual gaussian functions having the largest displacement from $z=0$ (i.e., the most-deflected beamlets) were centered at $\pm z_{\mathrm{max}}$. These sum-of-gaussians distributions represent the actual peak shapes that would be measured for the respective J values with $z_{\mathrm{max}}=100$ when the original peak shape is $P(z)$. At low J, fitting of Q^{FS} (z_0) to the true distribution by variation of z_{max} overestimates the actual value of z_{max} considerably. For example, for $J=1$ a value of $z_{\mathrm{max}}=144$ must be used in Eq. (A3) to obtain a Q^{FS} distribution that is in satisfactory agreement with the true $J=1$ distribution. Thus, fitting Q^{FS} to the measured peak shape for a $J=1$ system would lead to a $\sim$44% overestimation of z_{max} and thus of the magnetic moment [see Eq. (1)]. However, from Fig. 7 it can be seen that the ability of Q^{FS} to faithfully reproduce the shapes of the sum-of-gaussians distributions improves with increasing J: Applying this same test to the $J=2$ case, we find that the Q^{FS} fitting procedure overestimates the true moment by $\sim$11%, while for $J=4$ the error is $\sim$6%.

[1] F. J. Himpsel, J. E. Ortega, G. J. Mankey, and R. F. Willis, Adv. Phys. **47**, 511 (1998).
[2] A. J. Cox, J. G. Louderback, and L. A. Bloomfield, Phys. Rev. Lett. **71**, 923 (1993).
[3] A. J. Cox, J. G. Louderback, S. E. Apsel, and L. A. Bloomfield, Phys. Rev. B **49**, 12 295 (1994).
[4] K. Adachi, D. Bonnenberg, J. J. M. Franse, R. Gersdorf, K. A. Hempel, K. Kanematsu, S. Misawa, M. Shiga, M. B. Stearns, and H. P. J. Wijn, in *Landolt-Börnstein*, edited by H. P. J. Wijn (Springer-Verlag, Berlin, 1986), Vol. 19.
[5] L. A. Bloomfield, J. Deng, H. Zhang, and J. W. Emmert, in *Proceedings of the International Symposium on Cluster and Nanostructure Interfaces*, edited by P. Jena, S. N. Khanna, and B. K. Rao (World Publishers, Singapore, 2000), p. 131.
[6] W. A. de Heer (private communication).
[7] D. Hobbs, J. Hafner, and D. Spisak, Phys. Rev. B **68**, 014407 (2003).
[8] D. Hobbs, J. Hafner, and D. Spisak, Phys. Rev. B **68**, 014408 (2003).
[9] E. P. Wohlfarth, in *Ferromagnetic Materials*, edited by E. P. Wohlfarth (North-Holland, Amsterdam, 1980), Vol. 1, p. 1.
[10] S. Blundell, *Magnetism in Condensed Matter* (Oxford University Press, Oxford, 2001).
[11] M. B. Knickelbein, Phys. Rev. Lett. **86**, 5255 (2001).
[12] T. M. Briere, H. F. Sluiter, V. Kumar, and Y. Kawazoe, Phys. Rev. B **66**, 064412 (2002).
[13] P. Bobadova-Parvanova, K. Jackson, S. Srinivas, and M. Horoi, Phys. Rev. A **67**, 061202(R) (2003).
[14] S. N. Khanna, B. K. Rao, P. Jena, and M. B. Knickelbein, Chem. Phys. Lett. **378**, 374 (2003).
[15] M. B. Knickelbein, J. Chem. Phys. **116**, 9703 (2002).
[16] Materials Preparation Center (MPC), Ames Laboratory, Ames, Iowa. Ames Laboratory is a national laboratory operated for the U.S. Department of Energy (DOE) by Iowa State University under Contract No. W-7405-ENG-82. The MPC is supported by the Office of Basic Energy Sciences, Materials Science Division.
[17] G. M. Koretsky and M. B. Knickelbein, J. Chem. Phys. **106**, 9810 (1997).
[18] M. B. Knickelbein, S. Yang, and S. J. Riley, J. Chem. Phys. **93**, 94 (1990).
[19] B. A. Collings, A. Amrein, D. M. Rayner, and P. A. Hackett, J. Chem. Phys. **99**, 4174 (1993).
[20] D. McColm, Rev. Sci. Instrum. **37**, 1115 (1966).
[21] W. A. de Heer and P. Milani, Rev. Sci. Instrum. **62**, 670 (1991).
[22] W. A. de Heer, P. Milani, and A. Châtelain, Phys. Rev. Lett. **65**, 488 (1990).
[23] J. A. Becker and W. A. de Heer, Ber. Bunsenges. Phys. Chem. **96**, 1237 (1992).
[24] I. M. L. Billas, A. Châtelain, and W. A. de Heer, Science **265**, 1682 (1994).
[25] M. B. Knickelbein, Chem. Phys. Lett. **353**, 221 (2002).
[26] J. P. Bucher, D. C. Douglass, and L. A. Bloomfield, Phys. Rev. Lett. **66**, 3052 (1991).
[27] D. C. Douglass, A. J. Cox, J. P. Bucher, and L. A. Bloomfield, Phys. Rev. B **47**, 12 874 (1993).
[28] J. G. Louderback, A. J. Cox, L. J. Lising, D. C. Douglass, and L. A. Bloomfield, Z. Phys. D: At., Mol. Clusters **26**, 301 (1993).
[29] S. E. Apsel, J. W. Emmert, J. Deng, and L. A. Bloomfield, Phys. Rev. Lett. **76**, 1441 (1996).
[30] S. N. Khanna and S. Linderoth, Phys. Rev. Lett. **67**, 742 (1991).
[31] D. C. Douglass, J. P. Bucher, and L. A. Bloomfield, Phys. Rev. Lett. **68**, 1774 (1992).
[32] A. J. Cox, D. C. Douglass, J. G. Louderback, A. M. Spencer, and L. A. Bloomfield, Z. Phys. D: At., Mol. Clusters **26**, 319 (1993).
[33] J. P. Bucher and L. A. Bloomfield, Int. J. Mod. Phys. B **7**, 1079 (1993).
[34] P. Dugourd, I. Compagnon, F. Lepine, R. Antoine, D. Rayane, and M. Broyer, Chem. Phys. Lett. **336**, 511 (2001).
[35] N. F. Ramsey, *Molecular Beams* (Oxford University Press, Oxford, 1956).
[36] M. B. Knickelbein, A. Nakajima, and K. Miyajima (unpublished).
[37] G. F. Bertsch and K. Yabana, Phys. Rev. A **49**, 1920 (1994).
[38] J. P. Toennies and K. Winkelmann, J. Chem. Phys. **66**, 3965 (1977).
[39] G. M. McClelland, K. L. Senger, J. J. Valentini, and D. R. Herschbach, J. Phys. Chem. **83**, 947 (1979).
[40] A. Amirav, U. Even, and J. Jortner, Chem. Phys. **51**, 31 (1980).
[41] A. Maiti and L. M. Falicov, Phys. Rev. B **48**, 13 596 (1993).
[42] G. Bertsch, N. Onishi, and K. Yabana, Z. Phys. D: At., Mol. Clusters **34**, 213 (1995).
[43] V. Visuthikraisee and G. Bertsch, Phys. Rev. A **54**, 5104 (1996).
[44] G. Bertsch, N. Onishi, and K. Yabana, Surf. Rev. Lett. **3**, 435 (1996).
[45] N. Hamamoto, N. Onishi, and G. Bertsch, Phys. Rev. B **61**, 1336 (2000).
[46] The (dimensionless) magnetic susceptibilities are essentially equivalent in both both SI and cgs units, but differ by a factor of 4π, with $\chi_{SI}=4\pi\chi_{cgs}$. Here we use the SI definition.
[47] A. Châtelain, Philos. Mag. B **79**, 1367 (1999).
[48] M. R. Pederson, F. Reuse, and S. N. Khanna, Phys. Rev. B **58**, 5632 (1998).
[49] S. K. Nayak and P. Jena, Chem. Phys. Lett. **289**, 473 (1998).
[50] S. K. Nayak, B. K. Rao, and P. Jena, J. Phys.: Condens. Matter **10**, 10863 (1998).
[51] S. K. Nayak, M. Nooijen, and P. Jena, J. Phys. Chem. A **103**, 9853 (1999).
[52] R. J. Van Zee, C. A. Baumann, S. V. Bhat, and W. Weltner Jr, J. Chem. Phys. **76**, 5636 (1982).
[53] C. A. Baumann, R. J. Van Zee, S. V. Bhat, and W. Weltner Jr., J. Chem. Phys. **78**, 190 (1983).
[54] N. O. Jones, S. N. Khanna, T. Baruah, and M. R. Pederson (unpublished).
[55] G. Arfken, *Mathematic Methods for Physicists* (Academic Press, Boston, 1985).
[56] S. N. Khanna (private communication).